The impact of a magnetic ion on the thermoelectric properties of copper-rich quaternary selenides

JPhys Energy

The impact of a magnetic ion on the thermoelectric properties of copper-rich quaternary selenides

Journal of Physics: Energy

OPEN ACCESS

RECEIVED
22 December 2021

REVISED
4 April 2022

ACCEPTED FOR PUBLICATION
25 April 2022

PUBLISHED
12 May 2022

PAPER

The impact of a magnetic ion on the thermoelectric properties of copper-rich quaternary selenides

Alaa Aldowiesh, Panagiotis Mangelis, Paz Vaqueiro* and Anthony V Powell*

Department of Chemistry, University of Reading, Whiteknights, Reading RG6 6DX, United Kingdom
* Authors to whom any correspondence should be addressed.

E-mail: p.vaqueiro@reading.ac.uk **and** a.v.powell@reading.ac.uk

Keywords: thermoelectric, kesterite, stannite, selenide

Supplementary material for this article is available online

Abstract

A series of copper-based *p*-type chalcogenide semiconductors, $Cu_{2+x}BGe_{1-x}Se_4$ (B = Zn, Fe; $0 \leqslant x \leqslant 0.15$), was prepared by high-temperature methods, to explore the impact of replacement of the closed-shell ion, Zn^{2+}, with the magnetically active, Fe^{2+} cation. Powder x-ray diffraction in conjunction with Rietveld refinement reveals that zinc-containing materials are described in the kesterite-type structure (space group: $I\bar{4}$) and contain trace amounts of secondary phases, whereas in the iron analogues, described in the stannite-type structure (space group: $I\bar{4}2m$), single-phase behaviour persists to $x = 0.1$. Excess copper ions lead to the formation of holes and the electrical resistivity of both series is reduced from that of the stoichiometric end members. In the case of the iron-containing materials, this is shown to be due to an increase in the hole mobility, μ. This decrease in resistivity offsets the observed reduction in Seebeck coefficient and both series exhibit an improvement in thermoelectric performance. The lower electrical resistivity of the iron-containing materials, leads to higher figures-of-merit, compared to those of the zinc-containing materials at the same level of copper excess. The maximum figure-of-merit, $ZT = 0.3$ is attained for $Cu_{2.075}FeGe_{0.925}Se_4$ at the comparatively low temperature of 575 K. This is an increase of *ca*. 62% from that of the end member phase and *ca.* 67% higher than that of the zinc analogue at the same level of substitution.

1. Introduction

Thermoelectric generators are solid-state devices capable of directly converting heat to electricity. Such devices offer several advantages, including the absence of moving parts, high reliability and modularity. They have attracted attention in recent years owing to their potential for harvesting useful electrical energy from otherwise waste heat [1, 2]. It has been estimated [3] that one-third of worldwide energy consumption is associated with the industrial sector, with almost 50% considered waste heat. The implementation of thermoelectric energy recovery offers considerable scope to improve the efficiency of industrial processes, particularly those involving combustion of fossil fuels, thereby mitigating issues arising from increased energy demand and environmental problems associated with greenhouse gas emissions.

The performance of a thermoelectric material is determined by its transport properties and is embodied in a figure-of-merit, $ZT = S^2\sigma T/\kappa$, where T is the absolute temperature, S is the thermopower, σ is the electrical conductivity and κ is the total thermal conductivity, with contributions from both charge carriers (κ_e) and lattice vibrations (κ_L). Device efficiency is directly related to the figure-of-merit and therefore considerable efforts are being devoted to increase ZT, or perhaps more importantly the average figure-of-merit over the temperature range of operation of a device. Owing to the inter-dependence of the three key parameter, S, σ and κ, a number of strategies have been developed [4, 5] that seek to decouple the electrical and thermal transport properties, with the aim of either increasing the power factor ($S^2\sigma$) or reducing the lattice thermal conductivity (κ_L) in an effort to lower the total thermal conductivity ($\kappa = \kappa_e + \kappa_L$) [6].

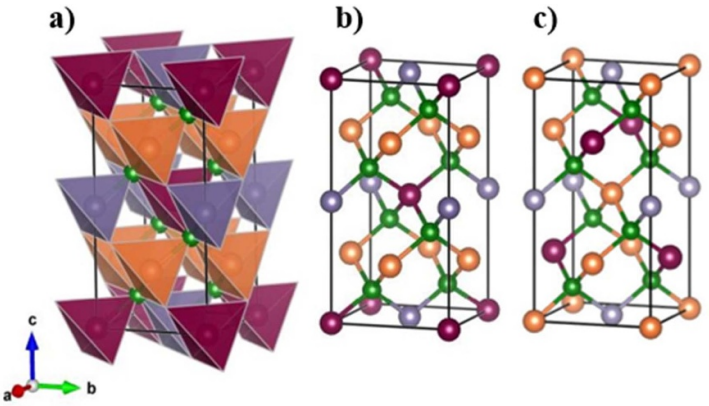

Figure 1. (a) Polyhedral representation of the stannite structure, ball and stick representation of (b) the stannite structure of $Cu_2FeGeSe_4$ and (c) the kesterite structure of $Cu_2ZnGeSe_4$. Copper-centred tetrahedra and atoms in orange, iron (in stannite), zinc (in kesterite) in violet, germanium and selenium atoms in wine and green respectively.

Commercial thermoelectric devices are based on Bi_2Te_3 [7]. However, maximum performance occurs near room temperature and material degradation occurs at elevated temperatures [8]. This, together with the low terrestrial abundance of tellurium makes Bi_2Te_3-based devices unsuitable for large-scale applications in energy harvesting in the mid-range of temperatures $373 \leqslant T/\mathrm{K} \leqslant 575$, where over 80% of industrial waste heat is released [3]. Recent efforts have therefore focused on creating alternative materials able to operate in this temperature regime. Among these, complex metal sulphides have emerged as promising candidates [1, 9]. Following the discovery of high thermoelectric performance in $Cu_{1.97}S$ [10] ($ZT = 1.7$ at 1000 K), copper-based chalcogenides have received considerable attention. Among these are the diamond-like materials which adopt what can be considered to be ordered derivatives of the zinc blende (sphalerite) structure [9]. Cation ordering gives rise to superstructures and is accompanied by a tetragonal distortion, which appears to have an impact on phonon propagation, thereby decreasing the lattice thermal conductivity [11].

The thermoelectric properties of quaternary diamond-like copper chalcogenides of general formula A_2BCQ_4 where (A = Cu; B = Zn, Fe, Co, Ni, Cd, Hg; C = Ge, Sn; Q = Se, S) have attracted particular interest [12–16]. These materials adopt tetragonal superstructures of zinc blende, in which there is a doubling of the unit-cell along the c-direction. Depending on the cation distribution, materials may adopt either the stannite ($I\bar{4}2m$) or kesterite ($I\bar{4}$) variants (figure 1). The similarity of the lattice parameters of the two forms, together with the lack of discrimination through systematic absences associated with the relevant space groups, results in considerable ambiguity over the structural description of a given material. The potential for cation disorder adds further complexity. A recent investigation [17] of A_2ZnBQ_4 (A = Cu, Ag; B = Sn, Ge; Q = S, Se) using a combination of neutron diffraction and Density-Functional Theory (DFT) simulations identifies kesterite as the structure adopted, albeit with partial cation ordering in the copper-containing phases. Introduction of an open-shell transition-metal ion may have an impact on the relative energies of the two alternatives, and the parent material, $Cu_2FeGeSe_4$, of the series investigated in this work, has been described in both the stannite and kesterite forms [18, 19]. Here, we adopt the description of Schäfer and Nitsche [20] and consider $Cu_2FeGeSe_4$ to adopt the stannite structure, (figure 1(b)), in which copper cations reside exclusively at 4d crystallographic sites resulting in copper layers at z = ¼ and ¾. This differs from the kesterite structure in which copper cations are located in all metal layers (figure 1(c)).

The bulk undoped materials $Cu_2ZnSnSe_4$ [12], $Cu_2MgSnSe_4$ [21] and $Cu_2CdSnSe_4$ [22] exhibit maximum values of the figure-of-merit of, $ZT = 0.28$, $ZT = 0.22$ and $ZT = 0.18$ respectively, at 700 K. Investigations of stannite and kesterite phases have focused on chemical substitution to tune the transport properties and hence optimize the thermoelectric response. Shi *et al* [12] have explored $Cu_2ZnSnSe_4$ as a potential thermoelectric material, despite its moderately large band gap ($E_g = 1.44$ eV), on the basis of its low lattice thermal conductivity. Partial replacement of tin by indium increases the hole carrier concentration, which results in a substantial reduction in the electrical resistivity. This is sufficient to compensate for the decrease in Seebeck coefficient, leading to an enhanced power factor. This, together with the retention of a low thermal conductivity on substitution, results in a maximum figure-of-merit, $ZT = 0.95$ for $Cu_2ZnSn_{0.9}In_{0.1}Se_4$ [12] at 850 K. Similarly, Liu *et al* [22] report a figure-of-merit $ZT = 0.65$ at 700 K in $Cu_{2.01}Cd_{0.9}SnSe_4$.

It has been proposed that the presence of a magnetic cation in the diamond-like semiconductors may increase the electrical conductivity, without having a deleterious impact on the Seebeck coefficient [23–25].

For example maximum figures-of-merit in the range $0.4 \leqslant ZT \leqslant 0.7$ have been reported for quaternary compounds, Cu_2BSnSe_4 (B = Fe, Co, Mn) [26], containing magnetic cations. Tsujii and Mori [27] have studied the impact of the effective mass on the Seebeck coefficient for magnetic thermoelectric materials in the n-type doped chalcopyrite derivatives, $Cu_{1-x}Fe_{1+x}S_2$ ($0 \leqslant x \leqslant 0.1$). Spin-polarised band structure calculations [28] reveal that the valence band in the region of the Fermi energy (E_F) has a large contribution from Fe-3d states, the spin of which contributes to the antiferromagnetic ordering. States at energies just above E_F are composed of Fe-3d states of the minority spin, antiparallel to the ordered moment. On the basis of these calculations, Tsujii and Mori [27] have suggested that interaction between charge carriers and the magnetic moment provides a mechanism for the observed increase in effective mass, m^*, at higher carrier concentrations, which leads to an enhanced Seebeck coefficient in doped phases.

Here, we have used copper substitution to tune the transport properties of quaternary chalcogenides containing a magnetic (Fe) or a non-magnetic (Zn) cation at the B-site through preparation of series of materials of general formula $Cu_{2+x}BGe_{1-x}Se_4$ (B = Fe, Zn; $0 \leqslant x \leqslant 0.15$). The results demonstrate that, while the thermoelectric properties in both series are enhanced by copper substitution, the presence of a magnetic cation (Fe) leads to higher performance. A maximum figure-of-merit, $ZT = 0.3$ is achieved for $Cu_{2.075}FeGe_{0.925}Se_4$ at 575 K. This represents *ca.* 62% increase over that of the stoichiometric end-member phase at this temperature and is *ca.* 67% higher than the maximum figure-of-merit ($ZT = 0.18$) attained in the analogous Zn-containing materials at this temperature, for the same level of copper excess.

2. Methods

Polycrystalline powders of materials with general formula $Cu_{2+x}BGe_{1-x}Se_4$ (B = Fe, Zn) were prepared by solid-state synthesis. Appropriate amounts of copper (Sigma-Aldrich, powder, 99.999%), iron (Sigma-Aldrich, powder, <10 μm, 99.9%), zinc (Sigma-Aldrich, powder, <150 μm, 99.995%), germanium (Sigma-Aldrich, powder, ⩾99.999%) and selenium (Sigma-Aldrich, pellets, <5 mm, ⩾99.99%) were ground using an agate pestle and mortar. The mixture was placed in a fused-silica tube that was then evacuated and sealed at 10^{-4} mbar. Mixtures containing iron were heated at 973 K for 48 h and those containing zinc at 923 K for the same duration. A heating and cooling rate of 2 °C min^{-1} was used in all cases. Preparation of $Cu_{2+x}ZnGe_{1-x}Se_4$ materials required a second firing, following grinding, at 1073 K for 96 h.

Powder x-ray diffraction data were collected on the as-prepared powders to assess phase purity before consolidation by hot pressing. Approximately 1 g of the as-prepared powder was placed in a graphite mould between two tungsten carbide dies. The surfaces of the dies were lined with graphite foil to avoid direct contact with the sample. Hot pressing of the iron-containing phases was carried out at 600 °C and 80 bar for 45 min. The pressure was reduced to 65 bar for consolidation of the zinc-containing materials. A flow of nitrogen was maintained during consolidation to prevent oxidation. After hot-pressing, any residue of graphite was removed from the surface of the pellets by polishing with silicon carbide paper. The resulting pellets have a diameter of 12.75 mm and thickness of 1.5 mm. The densities of the pellets were measured by the Archimedes' method, using an AE Adam PW 184 density balance. Sample densities in excess of 97% of the crystallographic density of the stoichiometric end member ($x = 0$) phases were achieved. Powder x-ray diffraction data were collected for the pellets, both before and after electrical and thermal transport property measurements.

Powder x-ray diffraction data were collected using a Bruker D8 Advance powder diffractometer, operating with Ge-monochromated CuKα_1 radiation, $\lambda = 1.5406$ Å, equipped with a LynxEye linear detector. Data for assessment of phase purity were collected over the angular range $10 \leqslant 2\theta/° \leqslant 120$ at room temperature, counting for 1 s at each increment of 0.0276° in the detector position. X-ray diffraction data, for the purposes of Rietveld refinement, were collected using a smaller step size (0.0066°, each for 1.2 s). Powder x-ray diffraction data were analysed by the Rietveld method, as implemented in the General Structure Analysis System (GSAS) program [29]. GSAS was used for the analysis of the diffraction data for the zinc-containing materials, while Rietveld refinements for the iron-containing materials were carried out using GSAS-II.

The Seebeck coefficient (S) and the electrical resistivity (ρ) data were measured simultaneously over the temperature range $300 \leqslant T/K \leqslant 625$ using a Linseis LSR3-800 instrument, under a 50 mbar pressure of He. Data were collected in steps of 10 K, using a current of 30 mA for four-probe resistivity measurements and a temperature gradient of 50 K for the determination of the Seebeck coefficient. Thermal diffusivity was measured over the temperature range $300 \leqslant T/K \leqslant 575$ in steps of 25 K using a Netzsch LFA 447 Nanoflash instrument. Measurements were conducted on the same pellets as used for the investigation of electrical transport properties. Prior to thermal transport measurements, the top and bottom surfaces of the pellets were spray-coated with a thin layer of graphite to maximize absorption and emission of radiation. The data were analysed using Cowan's model [30] with a pulse correction applied. The thermal conductivity was determined from the diffusivity data, using values of the heat capacity calculated using the Dulong–Petit

equation. The uncertainties in the values of the electrical resistivity, Seebeck coefficient and thermal conductivity are 5%, 5% and 10% respectively. Considering the combined uncertainties of all the measurements, the uncertainty in the calculation of figure-of-merit, ZT, is estimated to be *ca.* 15%. The Hall coefficient (R_H), carrier concentration (n_H) and Hall mobility (μ_H) were measured at room temperature for the $Cu_{2+x}FeGe_{1-x}Se_4$ phases by the van der Pauw method, using an Ecopia Hall Effect System HMS-3000. The circular pellet was cut into a square with dimensions of 5 mm^2 and secured to the sample board by four gold probes after adding silver paste to the four vertices of the sample. Thermogravimetric analysis (TGA) measurements for $Cu_2FeGeSe_4$ were carried out using a TA-TGA Q50 instrument. Approximately 20 mg of powder were placed in a pan made of alumina and heated under nitrogen flow up to 1123 K. Differential scanning calorimetry (DSC) data were collected using a TA- DSC Q2000 instrument, by heating *ca.* 5 mg of sample up to 1073 K.

3. Results and discussion

Powder x-ray diffraction data (figures S1 and S2 available online at stacks.iop.org/JPEnergy/4/034001/mmedia) for both series of materials are indexable on the basis of a tetragonal unit cell. Single phase behaviour is observed in $Cu_{2+x}FeGe_{1-x}Se_4$ to a composition with $x = 0.1$. At higher levels of copper substitution, trace amounts of the ternary chalcopyrite ($CuFeS_2$) are discernible, indicated by the appearance of intensity on the high-angle side of the most intense peaks (figure S1). However, peaks due to this secondary phase disappear on hot pressing, suggesting homogenization to a single phase with the original nominal composition occurs as the result of diffusion. In the analogous zinc-containing materials (figure S2) trace amounts of the binary selenides, ZnSe and CuSe are discernible at all compositions.

The tetragonal unit cell is consistent with the adoption of either a stannite- or a kesterite-type structure. However, as noted above, discrimination between these two structure types is not possible on the basis of powder x-ray diffraction alone. On the basis of our previous work utilising a combination of powder neutron diffraction and DFT [17], we hereafter describe materials of general formula $Cu_{2+x}ZnGe_{1-x}Se_4$ in a kesterite-type structure, whereas following the work of Schafer and Nitsche [20] phases of the form $Cu_{2+x}FeGe_{1-x}Se_4$ are described in the stannite-type structure. Rietveld refinements using powder x-ray diffraction data for as-prepared $Cu_{2+x}ZnGe_{1-x}Se_4$ ($0 \leqslant x \leqslant 0.15$) were therefore initiated in the space group $I\bar{4}$, using our previous results [17] from powder neutron diffraction for the initial structural model. Structural refinement of materials in the series $Cu_{2+x}FeGe_{1-x}Se_4$ ($0 \leqslant x \leqslant 0.15$) was initiated in the space group $I\bar{4}2m$, using data for $Cu_2FeGeSe_4$ [20] for the initial structural model.

In both series, for compositions with $x > 0$, additional copper cations, Cu(2), replace germanium cations at the 2*b* sites, with site occupancy factors set at values consistent with the nominal stoichiometry. The isotropic thermal parameters for cations at the 2*a* (Fe) and 2*b* (Ge/Cu) sites were constrained to be equal in refinements within the $Cu_{2+x}FeGe_{1-x}Se_4$ series, while in the case of $Cu_{2+x}ZnGe_{1-x}Se_4$, the thermal parameters of all sites were constrained to be equal. Backgrounds were fitted using a Chebyshev polynomial function. For materials of general formula $Cu_{2+x}FeGe_{1-x}Se_4$ a secondary chalcopyrite phase was introduced into the refinement for compositions with $x \geqslant 0.1$. Refinement indicates a maximum weight fraction for the chalcopyrite phase of *ca.* 7 wt.% in the as-prepared powders. In the case of the analogous zinc-containing materials, ZnSe and CuSe secondary phases were introduced into the refinements using data for the copper-rich compositions with maximum weight fractions of *ca.* 8.5 and 5.1 wt.% respectively. No changes were observed in the powder x-ray diffraction patterns of zinc-containing materials after hot pressing or following the electrical and thermal transport property measurements. Representative final observed, calculated and difference profiles for the end member ($x = 0$) phase and one copper-rich phase ($x = 0.075$) from each series are presented in figures 2 and 3, with the remaining profiles provided as supplementary information. Refined parameters are provided in tables S1 and S2 of the supplementary information.

The lattice parameters of the end-member phase, $Cu_2FeGeSe_4$, are consistent with those reported by Quintero *et al* [31] and by Zeier *et al* [19] although the *c* parameter is reduced slightly from that in the latter report. As formally Ge^{4+} is replaced with Cu^+, the in-plane parameter, *a*, decreases slightly (*ca.* 0.4%), while the *c*-parameter initially increases by a comparable amount before saturating at $x \geqslant 0.1$ (figure 4). The $c/2a$ ratio initially changes from <1.0 to a value that exceeds 1.0, thereafter decreasing towards unity with increasing copper excess, indicating that the tetragonal distortion is retained throughout the composition range. This is reflected in bond angles at the tetrahedral sites which show slight deviations from the ideal tetrahedral value. The bond distances and angles are provided in the supplementary information (tables S3 and S4).

Refined unit-cell parameters of the end-member phase $Cu_2ZnGeSe_4$ are in good agreement with previous reports [32]. The unit cell volume shows little change (an increase of <0.7%) on replacing iron with zinc, consistent with the similar ionic radii of the Zn^{2+} and Fe^{2+} cations [33]. The changes in lattice

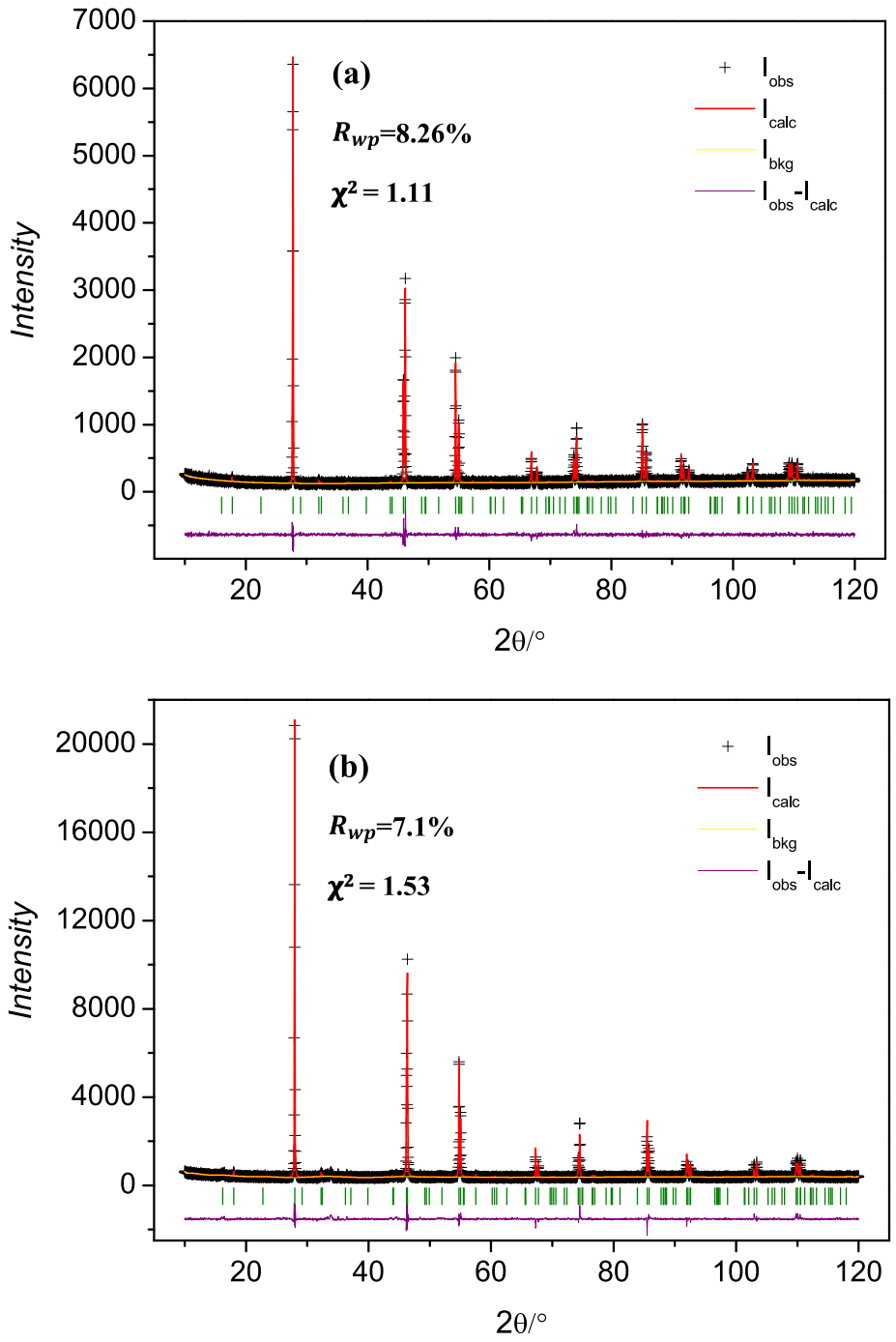

Figure 2. Final observed (crosses), calculated (full line) and difference (lower full line) profiles from Rietveld refinement in space group $I\bar{4}2m$ using powder x-ray diffraction data for (a) $Cu_2FeGeSe_4$ and (b) $Cu_{2.075}FeGe_{0.925}Se_4$. Reflection positions are marked.

parameters (figure 4) on copper substitution in the zinc-containing materials are less marked than in the $Cu_{2+x}FeGe_{1-x}Se_4$ series. The substitution of Ge by Cu causes some slight fluctuations in *a* and *c* lattice parameters, without affecting greatly the dimensions of the unit cell.

The resistivity of the end-member phase, $Cu_2FeGeSe_4$, shows marked thermal history dependence. After consolidation, $\rho(T)$ shows little variation on heating to *ca.* 570 K before decreasing sharply above this temperature (figure S11). This $\rho(T)$ dependence is similar to that reported by Raju *et al* [34] for the related phase $Cu_2ZnSnSe_4$. In order to investigate the unusual $\rho(T)$ behaviour of the as-consolidated material, repeated measurements of the resistivity on heating were conducted, allowing the sample to cool from 650 K to room temperature between measurements. On thermal cycling the resistivity in the region $300\ \text{K} \leqslant T/\text{K} \leqslant 575\ \text{K}$ drops by *ca.* 40% and the sharp decrease in resistivity at 575 K is gradually suppressed. The origin of this thermal history dependence is unclear. While complex chalcogenides often show compositional changes due to volatilization of the chalcogen during thermal treatment, thermogravimetric analysis (figure S12) reveals no significant weight loss (37.5%) until a temperature of 850 K is reached: a

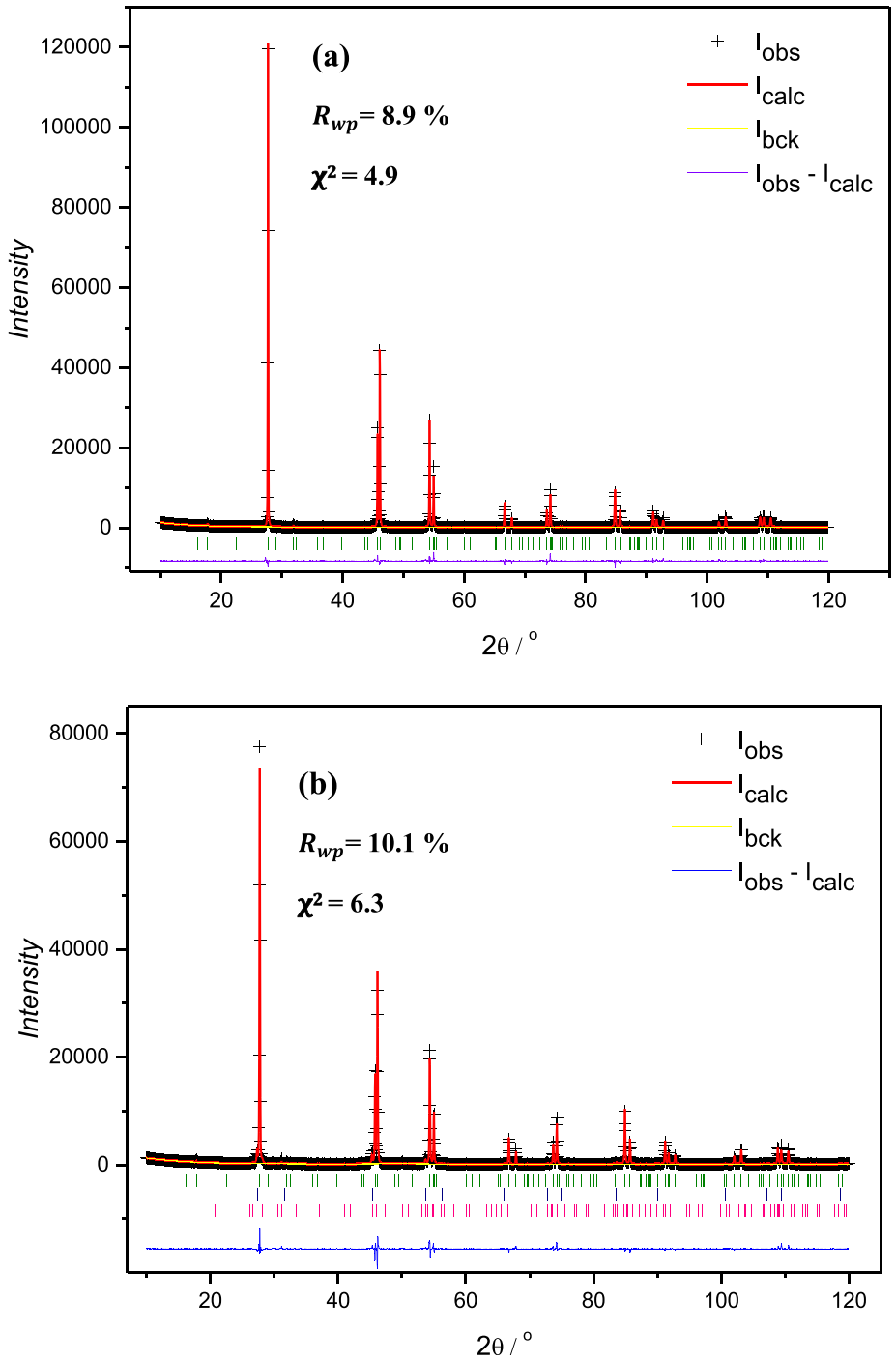

Figure 3. Final observed (crosses), calculated (full line) and difference (lower full line) profiles from Rietveld refinement in space group $I\bar{4}$ using powder x-ray diffraction data for (a) $Cu_2ZnGeSe_4$ (b) $Cu_{2.075}ZnGe_{0.925}Se_4$. Reflection positions for the principal kesterite phase, ZnSe and CuSe are indicated by green, navy and pink vertical markers respectively.

significantly higher temperature than where the changes in transport properties occur. Although evaporation of selenium from the analogous $Cu_2ZnGeSe_4$ [19] has been observed in DSC data collected under a dynamic vacuum at lower temperatures, the temperature (723 K) is above that at which the thermal history dependence of the transport properties of $Cu_2FeGeSe_4$ are observed. In the kesterite-type phase, Cu_2ZnSnS_4, a low-temperature order-disorder phase transition, involving disordering of Cu and Zn cations and the concomitant formation of Cu/Zn antisite defects, occurs at 533 K [35]. The degree of order in a given sample is dependent on the rate of cooling [35]. It has been established that Cu/Zn disorder is responsible for a significant reduction in the band gap [36]. Similarly, annealing of kesterite $Cu_2ZnSnSe_4$ thin films below the temperature of the order-disorder phase transition, increases the band gap by 110 meV when compared to that of the fully disordered material [37, 38]. The order-disorder phase transition in kesterite-type phases is accompanied by a marked anomaly in $\rho(T)$ and by a weak feature in DSC data [39]. Moreover, DSC data for

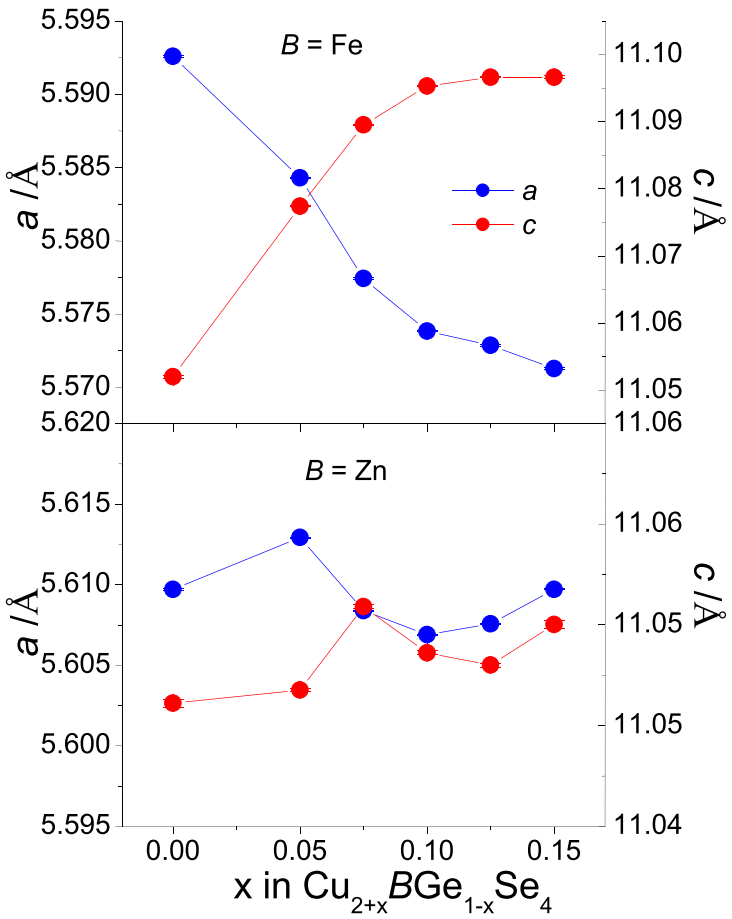

Figure 4. Refined lattice parameters a and c, for $Cu_{2+x}BGe_{1-x}Se_4$ ($0 \leqslant x \leqslant 0.15$) with B = Fe (upper plot); B = Zn (lower plot). Error bars lie within the points.

Cu_2FeGeS_4 also shows a weak feature between 520 K and 580 K, of unknown origin [40]. Our DSC data for $Cu_2FeGeSe_4$ (figure S13) shows a similar anomaly, between 510 K and 530 K. Taken together, these observations suggest that the sudden drop in electrical resistivity of $Cu_2FeGeSe_4$ at *ca.* 570 K observed in this work (figure S11) is related to an order-disorder transition, involving the Cu and Fe cations. The degree of ordering of Cu and Fe cations determines the bandgap and hence the electrical resistivity. Repeated heating and cooling during the electrical transport property measurements is likely to reduce the degree of Cu/Fe ordering, hence decreasing the band gap and lowering the electrical resistivity.

The resistivity of $Cu_{2+x}Fe_{1-x}GeSe_4$ ($0.05 \leqslant x \leqslant 0.1$), shows a relatively weak temperature dependence, similar to the behaviour reported by Song *et al* [41] for the tin-containing analogues, $Cu_{2+x}Fe_{1-x}SnSe_4$, at a comparable level of copper excess. At higher levels of copper incorporation ($x = 0.125$ and 0.15), there is a more marked decrease in resistivity with increasing temperature, similar to the behaviour reported by Raju *et al* [34] for the series $Cu_{2+x}ZnSn_{1-x}Se_4$, described in the stannite structure. The replacement of what is formally Ge^{4+} with copper, requires partial oxidation of the latter to maintain charge balance, thereby creating holes in the copper valence band. However, in the case of the Cu rich materials reported here, the reduction of the resistivity in copper-rich phases (figure 5(a)), appears to derive primarily from an increase in the mobility, μ (table 1).

The change in the sign of $d\rho/dT$ that occurs above *ca.* 575 K for all $Cu_{2+x}Fe_{1-x}GeSe_4$ phases containing excess copper ($x > 0$) indicates a change to a metallic temperature dependence of the resistivity at high temperatures. A more marked manifestation of this is provided by the electrical resistivity data of the zinc-containing analogues (figure 5(b)). At *ca.* 475 K, the temperature dependence of the resistivity of the stoichiometric phase, $Cu_2ZnGeSe_4$, changes from a semiconducting to metallic-like temperature dependence. Similar anomalies have been observed previously by Zeier *et al* [42] in the copper rich samples, $Cu_{2+x}Zn_{1-x}SnSe_4$, and DSC also reveals an exothermic effect at around 450 K. It has been suggested [42] that this anomaly in electrical transport properties is associated with a semiconductor to metal transition on heating. However, the recent powder neutron diffraction work of Mangelis *et al* [39] reveals that the anomalies in the electron-transport properties coincide with structural changes involving a second-order phase transition. In particular, disordering of Cu and Zn cations from an initially partially ordered

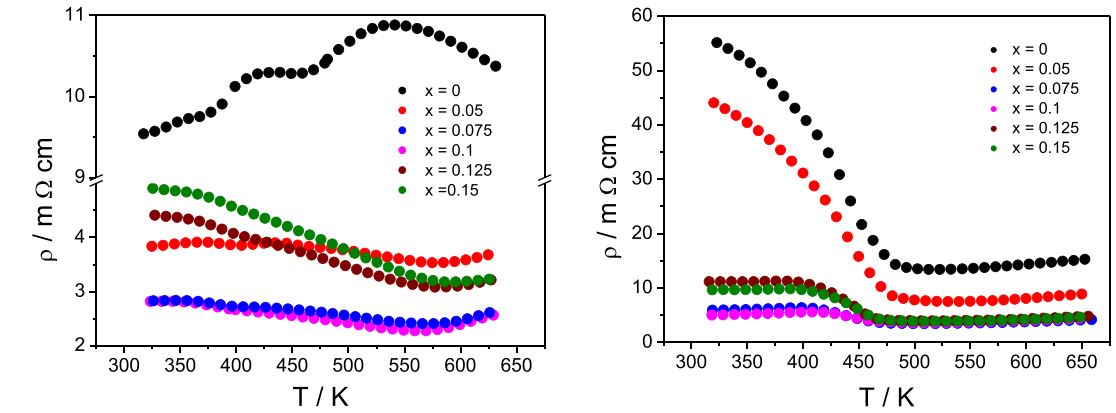

Figure 5. Resistivity as a function of temperature for all samples in the series (a) $Cu_{2+x}FeGe_{1-x}Se_4$ ($0 \leqslant x \leqslant 0.15$) (b) $Cu_{2+x}ZnGe_{1-x}Se_4$ ($0 \leqslant x \leqslant 0.15$).

Table 1. Hall coefficient R_H, the Hall carrier concentration and mobility for samples in the series $Cu_{2+x}FeGe_{1-x}Se_4$ ($0 \leqslant x \leqslant 0.15$).

Nominal composition	R_H ($cm^3\,C^{-1}$)	n_p (cm^{-3})	μ ($cm^{-2}\,V^{-1}\,s^{-1}$)
$Cu_2FeGeSe_4$	$7.8(1) \times 10^{-2}$	$9.2(1) \times 10^{19}$	6.8(2)
$Cu_{2.05}FeGe_{0.95}Se_4$	$8.0(2) \times 10^{-2}$	$8.1(3) \times 10^{19}$	17.9(6)
$Cu_{2.075}FeGe_{0.925}Se_4$	$4.3(2) \times 10^{-1}$	$1.5(5) \times 10^{19}$	130(2)
$Cu_{2.1}FeGe_{0.9}Se_4$	$5.5(6) \times 10^{-1}$	$1.1(3) \times 10^{19}$	169(6)
$Cu_{2.125}FeGe_{0.875}Se_4$	$2.7(2) \times 10^{-2}$	$2.4(2) \times 10^{20}$	5.4(2)
$Cu_{2.15}FeGe_{0.85}Se_4$	$4.9(3) \times 10^{-2}$	$1.3(2) \times 10^{20}$	8.8(1)

arrangement to a fully disordered state, is accompanied by partial melting of the copper sub-lattice, resulting in delocalization of copper cations at the 2*c* and 2*d* positions occupied by Cu and Zn, and at the 2*a* site occupied exclusively by Cu. The substitution of germanium by copper in the series $Cu_{2+x}ZnGe_{1-x}Se_4$ reduces the resistivity while also suppressing the electronic signature of the phase transition, notably at $x \geqslant 0.075$. This may be associated with an increase in the defect formation energy for the creation of copper vacancies (V_{Cu}) with increasing copper content. This would be consistent with the calculations of Song *et al* [41] who have shown that there is a significant increase in the defect formation energy for negatively charged V_{Cu} defects in copper-rich $Cu_{2+x}Fe_{1-x}SnSe_4$, phases. Charge balancing considerations again require the creation of holes in the valence band as the result of substitution of germanium with copper. The reduction in resistivity is most marked at compositions corresponding to $x = 0.075$ and $x = 0.1$, suggesting these are in the region of the optimum level of hole doping. Unfortunately, it did not prove possible to obtain reliable Hall coefficient data for these materials.

The Seebeck coefficient for all members of the two series reported here is positive over the whole range of temperature (figure 6), indicating that the majority charge carriers are holes at all compositions. In the case of $Cu_{2+x}FeGe_{1-x}Se_4$ this is also consistent with the sign of the Hall coefficient (table 1). By contrast with the marked thermal history dependence of the resistivity of the end-member phase, $Cu_2FeGeSe_4$, the $S(T)$ behaviour of the non-stoichiometric phases remains broadly similar on cycling. The Seebeck coefficient of materials in the series $Cu_{2+x}FeGe_{1-x}Se_4$ ($0 \leqslant x \leqslant 0.15$) increases with increasing temperature, with a slight fluctuation in the region around 550 K, above which it exhibits a near linear temperature dependence (figure 6(a)). This, together with the metallic-like $\rho(T)$ behaviour above *ca.* 550 K, suggests the materials are degenerate semiconductors at elevated temperatures. Increasing the copper content leads to a reduction in the magnitude of the Seebeck coefficient, which is consistent with the reduction in resistivity. The Seebeck coefficient of materials $Cu_{2+x}ZnGe_{1-x}Se_4$ shows a similar reduction with increasing copper content suggesting it may have the same origin. The change in electrical transport properties evidenced in the $\rho(T)$ behaviour also manifests itself in the non-stoichiometric compositions in anomalies in $S(T)$ behaviour at temperatures in the range $450 \leqslant T/K \leqslant 500$. In a similar manner to the $\rho(T)$ behaviour discussed above, the signature of the transition in $S(T)$ in the series $Cu_{2+x}ZnGe_{1-x}Se_4$ is greatly suppressed with increasing x, owing to the greater difficulty of creating V_{Cu} defects in copper-rich phases.

Hall effect measurements (table 1) reveal a relatively low charge-carrier concentration in the end-member phase $Cu_2FeGeSe_4$, comparable with that reported Zeier *et al* [19] (7×10^{19} cm^{-3}) which is

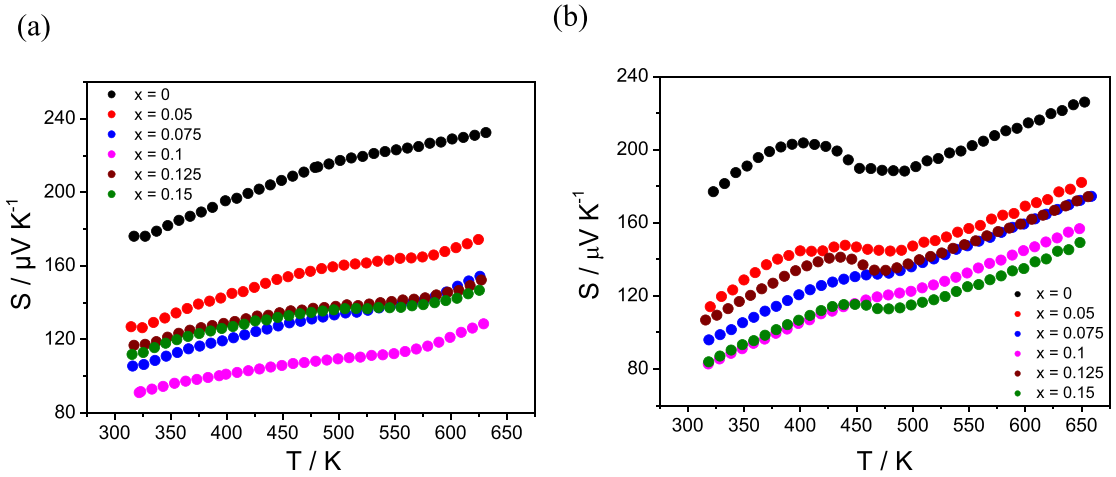

Figure 6. The Seebeck coefficient as a function of temperature for all samples in the series (a) $Cu_{2+x}FeGe_{1-x}Se_4$ ($0 \leqslant x \leqslant 0.15$) (b) $Cu_{2+x}ZnGe_{1-x}Se_4$ ($0 \leqslant x \leqslant 0.15$).

consistent with the relatively high Seebeck coefficient. Surprisingly, the carrier concentration remains low in the copper-rich compositions, initially dropping with increasing copper content, before reaching slightly higher values in materials with $x \geqslant 0.125$. This suggests that ionization of defects has a greater impact on carrier concentration than copper substitution and may lie behind the apparent non-systematic compositional variation of properties as has been reported in analogous series [19]. The mobility of $Cu_{2+x}FeGe_{1-x}Se_4$ shows a greater dependence on composition, increasing markedly by two orders of magnitude as x increases to 0.1, before returning to values comparable to that of the end-member phase at higher copper contents. It should be noted that for compositions with $x > 0.1$, materials contain small amounts of chalcopyrite (figure S1). A similar increase in mobility with increasing copper content to that observed for $x \leqslant 0.1$ has been reported by Song *et al* for the analogous tin-containing series, $Cu_{2+x}Fe_{1-x}SnSe_4$ [41] for which calculations indicate that in the end-member, $Cu_2FeSnSe_4$, the lowest defect formation energy is associated with the creation of copper vacancies V_{Cu}. Moreover, their negative formation energy suggests that V_{Cu} can be formed spontaneously during thermal processing. The copper vacancies perturb the periodicity and introduce additional impurity scatterers, which contribute to the low mobility ($\mu = 6.76$ cm^2 V^{-1} s^{-1} at 300 K) of the end-member phase (table 1), while holes associated with the formation of V_{Cu} accounts for the *p*-type behaviour of the nominally stoichiometric phase. However, the calculations also reveal that the formation of negatively charged copper defects is suppressed in copper-rich phases while anti-site defects become favoured. In the series $Cu_{2+x}FeGe_{1-x}Se_4$ ($0 \leqslant x$ 0.15), excess copper is also likely to suppress the creation of V_{Cu} defects, thereby reducing the number of scattering centres and leading to the increase in mobility at levels of copper substitution that extend to $x = 0.1$. At higher levels of copper substitution, other defect states, including Cu_{Ge} and Cu_{Fe} will play a more prominent role in scattering charge carriers, leading to a fall in mobility. The initial increase in mobility, without a correspondingly marked change in carrier concentration, results in the resistivity being reduced substantially without adversely affecting the Seebeck coefficient, for which values in the range 140−115 μv K^{-1} are observed at 575 K (for compositions with $x = 0.075$, 0.1). This results in an improvement in the power factor (figure 7(a)) in copper-rich phases, with the highest values being observed for compositions with $0.05 \leqslant x \leqslant 0.075$, suggesting the optimum level of substitution lies in this range. A similar conclusion may be drawn from the data for the series $Cu_{2+x}ZnGe_{1-x}Se_4$, for which the highest power factor is observed at the same level of substitution ($x = 0.075$). However, the maximum power factor, $S^2\sigma = 9.12$ μW cm^{-1} K^{-2} determined for $Cu_{2.075}FeGe_{0.925}Se_4$ at 625 K, is *ca* 30% larger than that for the analogous zinc-containing phase ($S^2\sigma = 6.9$ μW cm^{-1} K^{-2}) at the same temperature and level of substitution (figure 7(b)).

In contrast with the significant thermal history dependence of the electrical-transport property data, the thermal conductivity of $Cu_2FeGeSe_4$ at 575 K increases only slightly from $\kappa = 1.2$ W m^{-1} K^{-1} to $\kappa = 1.44$ W m^{-1} K^{-1} on cycling (figure S14). These values are comparable with those previously reported for the stoichiometric phase [19]. The contrast between the sensitivity of the electrical transport properties on thermal cycling and the somewhat invariant thermal conductivity is associated with the small contribution (<1%) made by the charge-carrier component, κ_e, to the total thermal conductivity. The total thermal conductivity shows a relatively weak dependence on the amount of excess copper ions, with the spread in values for phases with $x > 0$ lying in the range of 10%–20% (figure 8). This contrasts with the behaviour of

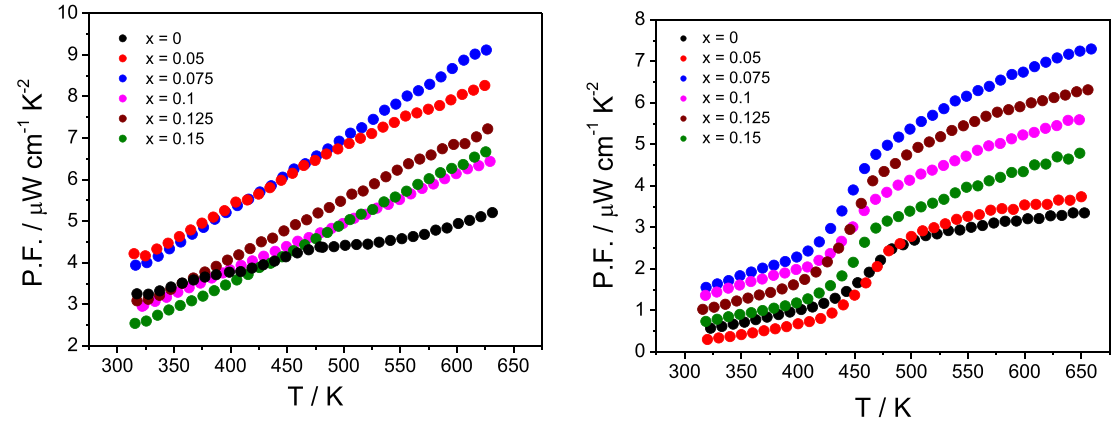

Figure 7. The power factor as a function of temperature for all samples in the series (a) $Cu_{2+x}FeGe_{1-x}Se_4$ ($0 \leqslant x \leqslant 0.15$) (b) $Cu_{2+x}ZnGe_{1-x}Se_4$ ($0 \leqslant x \leqslant 0.15$).

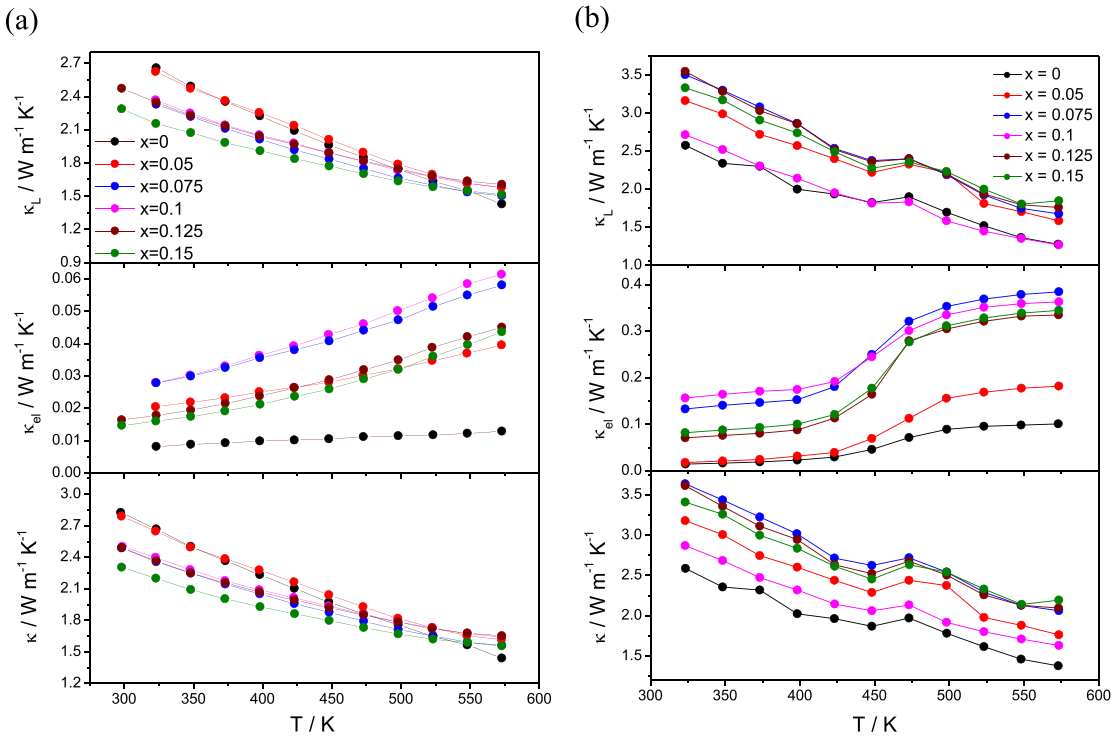

Figure 8. The total, lattice, and electronic thermal conductivity as a function of temperature for (a) $Cu_{2+x}FeGe_{1-x}Se_4$ ($0 \leqslant x \leqslant 0.15$) (b) $Cu_{2+x}ZnGe_{1-x}Se_4$ ($0 \leqslant x \leqslant 0.15$).

$Cu_{2+x}ZnGe_{1-x}Se_4$, which although exhibiting a comparable thermal conductivity in the stoichiometric ($x = 0$) phase ($\kappa = 1.4$ W m^{-1} K^{-1} at 575 K), shows a greater compositional dependence, with values in excess of $\kappa = 3.5$ W m^{-1} K^{-1} at 325 K and 2 W m^{-1} K^{-1} at 573 K being reached. Consequently, the thermal conductivity throughout the series $Cu_{2+x}ZnGe_{1-x}Se_4$ is significantly higher than for the iron-containing analogues. Similarly higher values of thermal conductivity have been reported by Raju *et al* [34] for the tin congeners $Cu_{2+x}ZnSn_{1-x}Se_4$. The thermal conductivities of phases containing closed-shell ions are significantly larger than for those containing the open-shell Fe^{2+} ion (for example, $\kappa = 1.57$ W m^{-1} K^{-1} for $Cu_{2.075}FeGe_{0.925}Se_4$, $\kappa = 2.07$ W m^{-1} K^{-1} for $Cu_{2.075}ZnGe_{0.925}Se_4$) and $\kappa = 2.52$ W m^{-1} K^{-1} for $Cu_{2.075}ZnSn_{0.925}Se_4$ at 575 K. Given the negligible mass difference between iron and zinc, the reduction in thermal conductivity is unlikely to be associated with mass-fluctuation scattering. However, it has been suggested [19, 25] that in contrast to a main-group closed-shell cation, an open-shell ion has a strong lattice anharmonicity which increases the Umklapp phonon–phonon scattering.

The replacement of Zn^{2+} with the open-shell magnetic ion, Fe^{2+} also has an impact on the electrical-transport properties, although the comparison is affected by the presence of the phase-transition at *ca*. 475 K in $Cu_{2+x}ZnGe_{1-x}Se_4$. Below this temperature, the resistivity of the iron-containing materials is generally lower than for the zinc congeners at a given level of substitution. The Seebeck coefficient of $Cu_2FeGeSe_4$ following the fourth measurement cycle (225 μV K^{-1} at 575 K), is comparable with that reported by Zeier *et al* [19] (230 μV K^{-1}) and is the same as the value determined here for $Cu_2ZnGeSe_4$ (225 μV K^{-1}), although Chetty *et al* [32] have reported a somewhat lower value 160 μV K^{-1} for $Cu_2ZnGeSe_4$.

Consideration of the band structure determined for the analogous stoichiometric $Cu_2FeSnSe_4$ stannite-structured phase [41] indicates that the states near the top of the valence band are primarily Se-*p* and Cu-*d* in character. Consequently, charge transport in *p*-type materials will be more affected by defects associated with copper and selenium sites, which would impair mobility, than by those associated with iron, as electronic states from the latter contribute to the conduction band minimum. Consequently, as the formation of V_{Cu} is suppressed through the introduction of excess copper on substitution of germanium by copper, the mobility is expected to increase, even against a background of increasing anti-site defects, Cu_{Ge}, as the electronic states of germanium make little contribution to the band structure in the vicinity of E_F. The introduction of defects plays an important role in phonon scattering processes and is also likely to be a significant contributor to the observed reductions in thermal conductivity.

Although band structure calculations have been carried out [19] for both end-member phases investigated here, in each case calculations were carried out for the alternative structure type ($Cu_2FeGeSe_4$, kesterite; $Cu_2ZnGeSe_4$, stannite) to that considered here. These calculations reveal differences near the top of the valence band between the stannite and kesterite forms. In particular the degeneracy in the region of the valence band maximum (VBM) is structure dependent, changing from a two-fold degeneracy in the stannite-structured $Cu_2ZnGeSe_4$ to a single parabolic band (SPB) in kesterite-structured $Cu_2FeGeSe_4$. However, in the iron-containing material there is a second four-fold degenerate band of Fe-*d* character lying *ca*. 82 meV lower than the VBM, with a much heavier effective mass of 1.91m_e. It has been suggested that this band could contribute to electron transport owing to its proximity to the VBM. A similar lower lying feature is observed in the band structure of the stannite-structured $Cu_2FeSnSe_4$ [41], suggesting its presence is not dependent on the structure type. The presence of an analogous Fe-*d* band located close to the VBM in the band structure of stannite-type $Cu_2FeGeSe_4$ investigated here would be expected to make a similar contribution to electronic transport, accounting for the relatively high electrical conductivity.

Tsujii and Mori [27] have suggested that the presence of a magnetic ion in chalcopyrite-related phases, leads to an increase in effective mass, through interaction of the carriers with the magnetic moment, resulting in an enhanced Seebeck coefficient. In the SPB approximation the Seebeck coefficient can be related to the effective mass (m^*) and charge-carrier concentration (n) through:

$$S = \frac{8\pi^2 k_B^2}{3eh^2}\left(\frac{\pi}{3n}\right)^{2/3} m^* T$$

where k_B, *e, h* and T are the Boltzmann constant, electron charge, Planck's constant and absolute temperature respectively. Using the values of the Seebeck coefficient and charge-carrier density determined for $Cu_2FeGeSe_4$, results in an estimated effective mass of $m^* = 1.8\ m_e$. This is larger than the value of 1.2 m_e determined by Zeier *et al* [42], for the zinc analogue, $Cu_2ZnGeSe_4$. The increase of 50% in effective mass in the material containing an open-shell cation, suggests an interaction between the charge carrier and the magnetic moment of the Fe^{2+} cation, similar to that reported by Tsujii and Mori for chalcopyrite-related materials [27]. Although m^* is greater (3.5–5.6 m_e depending on composition) in the latter, this may reflect the fact that the kesterite-type phases investigated here are magnetically more dilute (12.5 at.%) than the chalcopyrite phases reported in the earlier work (25 at%).

The presence of a magnetic ion in $Cu_{2+x}FeGe_{1-x}Se_4$ may be responsible for the maintenance of a relatively high Seebeck coefficient, despite the marked reduction in resistivity with increasing copper content. However, Xiao *et al* [25] have suggested that the degeneracy of the d^n electronic configuration of a magnetic ion may also play a role. The resulting spin entropy provides a mechanism for the enhancement of the Seebeck coefficient. Magnetic ions also alter the degeneracy of the electronic configurations, creating a more complex band structure. This may contribute to an increased mobility, which enhances the electrical conductivity. There is less evidence of an impact of spin entropy on the magnitude of the Seebeck coefficient on replacement of zinc in $Cu_2ZnGeSe_4$ by iron. However, spin-entropy may play a role in the maintenance of a relatively large Seebeck coefficient in copper-rich materials with increased electrical conductivity. This combination results in an increase of *ca.* 30% in the power factor on replacing the closed-shell ion, Zn^{2+}, with the magnetic ion, Fe^{2+} (figure 7).

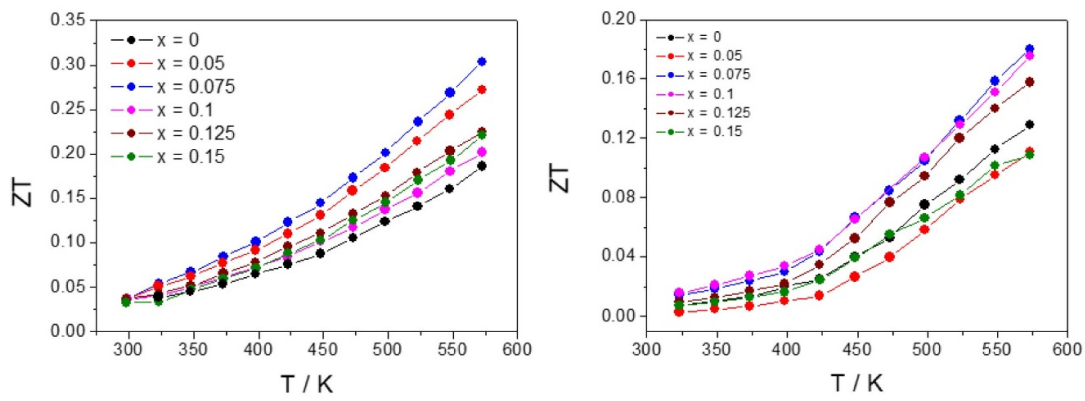

Figure 9. The figure-of-merit as a function of temperature for all samples in the series (a) $Cu_{2+x}FeGe_{1-x}Se_4$ ($0 \leqslant x \leqslant 0.15$) (b) $Cu_{2+x}ZnGe_{1-x}Se_4$ ($0 \leqslant x \leqslant 0.15$).

The figure-of-merit of the end-member phase $Cu_2FeGeSe_4$ (figure S14) increases slightly from $ZT = 0.13$ to $ZT = 0.19$ at 575 K, on thermal cycling, primarily as a result of the reduction in electrical resistivity. The figure-of-merit for $Cu_2FeGeSe_4$ at 575 K is comparable with that reported by Zeier *et al* [19] ($ZT = 0.14$) at this temperature and is higher than for analogues containing non-magnetic cations [32, 34]. This is also consistent with observations here that the maximum figure-of-merit of $Cu_2ZnGeSe_4$ ($ZT = 0.13$ at 575 K) is slightly lower than that of the iron-containing analogue. While substitution of germanium by copper increases the figure-of-merit in both non-stoichiometric series (figure 9), the impact is greater in the iron-containing series, which exhibits a maximum figure-of-merit $ZT = 0.3$ at 575 K for a composition at $x = 0.075$. This compares with a maximum value, $ZT = 0.18$, at the same temperature for the zinc-containing analogues, representing an increase of *ca*. 66% of $Cu_{2.075}BGe_{0.925}Se_4$ on moving from B = Zn to B = Fe. Significantly the highest figure-of-merit is observed at the same level of copper excess in both series.

4. Conclusions

In conclusion, we demonstrate that materials, $Cu_{2+x}BGe_{1-x}Se_4$ (B = Zn, Fe; $0 \leqslant x \leqslant 0.15$), are able to tolerate appreciable levels of substitution of germanium by copper. Materials containing excess copper show marked reductions in electrical resistivity, leading an increase in thermoelectric power factor. The increase is more marked in non-stoichiometric materials containing the magnetic iron, Fe^{2+}. The enhancement in power factor offsets the larger thermal conductivity that is seen in both series, and is sufficient to increase the figure-of-merit. The figure-of-merit of the iron-containing materials reaches a maximum value of $ZT = 0.3$ at 575 K for a composition at $x = 0.075$. This is *ca*. 66% higher than the maximum value attained in the analogous zinc-containing series. Interestingly, the maximum figure-of-merit in both series is achieved at the same level of copper substitution, suggesting this corresponds to the optimum doping level.

Data availability statement

All data that support the findings of this study are included within the article (and any supplementary files).

Acknowledgments

The authors would like to thank EPSRC (Award Ref. 1367504) and the University of Reading for financial support for P M, and for access to the Chemical Analysis Facility for powder x-ray diffraction and TGA/DSC measurements. A A would like to acknowledge the PhD funding provided by the Saudi Cultural Bureau.

ORCID iDs

Panagiotis Mangelis https://orcid.org/0000-0001-5948-1177
Paz Vaqueiro https://orcid.org/0000-0001-7545-6262
Anthony V Powell https://orcid.org/0000-0002-9650-1568

References

[1] Freer R and Powell A V 2020 Realising the potential of thermoelectric technology: a roadmap *J. Mater. Chem.* C **8** 441–63
[2] Shi X-L, Zou J and Chen Z-G 2020 Advanced thermoelectric design: from materials and structures to devices *Chem. Rev.* **120** 7399–515
[3] Takenobu K 2005 Thermoelectric power generation system recovering industrial waste heat *Thermoelectrics Handbook Macro to Nano* (Boca Raton: CRC Press) pp 50–51
[4] Tan G, Zhao L-D and Kanatzidis M G 2016 Rationally designing high-performance bulk thermoelectric materials *Chem. Rev.* **116** 12123–49
[5] Powell A V and Vaqueiro P 2017 Chalcogenide thermoelectric materials *Thermoelectric Materials and Devices, RSC Energy and Environment Series* (Cambridge: The Royal Society of Chemistry) pp 27–59
[6] Sootsman J R, Chung D Y and Kanatzidis M G 2009 New and old concepts in thermoelectric materials *Angew. Chem., Int. Ed.* **48** 8616–39
[7] Witting I T, Chasapis T C, Ricci F, Peters M, Heinz N A, Hautier G and Snyder G J 2019 The thermoelectric properties of bismuth telluride *Adv. Electron. Mater.* **5** 1800904
[8] Jiang C, Feng B, Hu J, Xiang Q, Li G, Li Y and He Z 2017 Thermal stability of p-type polycrystalline Bi_2Te_3-based bulks for the application on thermoelectric power generation *J. Alloys Compd.* **692** 885–91
[9] Powell A V 2019 Recent developments in Earth-abundant copper-sulfide thermoelectric materials *J. Appl. Phys.* **126** 100901
[10] He Y, Day T, Zhang T, Liu H, Shi X, Chen L and Snyder G J 2014 High thermoelectric performance in non-toxic earth-abundant copper sulfide *Adv. Mater.* **26** 3974–8
[11] Qiu P, Shi X and Chen L 2016 Cu-based thermoelectric materials *Energy Storage Mater.* **3** 85–97
[12] Shi X, Huang F, Liu M and Chen L 2009 Thermoelectric properties of tetrahedrally bonded wide-gap stannite compounds $Cu_2ZnSn_{1-x}In_xSe_4$ *Appl. Phys. Lett.* **94** 122103
[13] Coughlan C, Ibanez M, Dobrozhan O, Singh A, Cabot A and Ryan K M 2017 Compound copper chalcogenide nanocrystals *Chem. Rev.* **117** 5865–6109
[14] Xiong Q, Xie D, Wang H, Wei Y, Wang G, Wang G, Liao H, Zhou X and Lu X 2021 Colloidal synthesis of diamond-like compound Cu_2SnTe_3 and thermoelectric properties of $(Cu_{0.96}InTe_2)_{1-x}(Cu_2SnTe_3)_x$ solid solutions *Chem. Eng. J.* **422** 129985
[15] Zhang Q, Xi L, Zhang J, Wang C, You L, Pan S, Guo K, Li Z and Luo J 2021 Influence of Ag substitution on thermoelectric properties of the quaternary diamond-like compound $Zn_2Cu_3In_3Te_8$ *J. Materiomics* **7** 236–43
[16] Song Q, Qiu P, Zhao K, Deng T, Shi X and Chen L 2019 Crystal structure and thermoelectric properties of $Cu_2Fe_{1-x}Mn_xSnSe_4$ diamond-like chalcogenides *ACS Appl. Energy Mater.* **3** 2137–46
[17] Mangelis P, Aziz A, de Silva I, Grau-Crespo R, Vaqueiro P and Powell A V 2019 Understanding the origin of disorder in kesterite-type chalcogenides A_2ZnBQ_4 (A = Cu, Ag; B = Sn, Ge; Q = S, Se): the influence of inter-layer interactions *Phys. Chem. Chem. Phys.* **21** 19311–7
[18] Schorr S 2007 Structural aspects of adamantine like multinary chalcogenides *Thin Solid Films* **515** 5985–91
[19] Zeier W G, Pei Y, Pomrehn G, Day T, Heinz N, Heinrich C P, Snyder G J and Tremel W 2013 Phonon scattering through a local anisotropic structural disorder in the thermoelectric solid solution $Cu_2Zn_{1-x}Fe_xGeSe_4$ *J. Am. Chem. Soc.* **135** 726–32
[20] Schäfer W and Nitsche R 1974 Tetrahedral quaternary chalcogenides of the type Cu_2 II IVS_4 (Se_4) *Mater. Res. Bull.* **9** 645–54
[21] Pavan Kumar V, Guilmeau E, Raveau B, Caignaert V and Varadaraju U 2015 A new wide band gap thermoelectric quaternary selenide $Cu_2MgSnSe_4$ *J. Appl. Phys.* **118** 155101
[22] Liu M L, Chen I W, Huang F Q and Chen L D 2009 Improved thermoelectric properties of Cu-doped quaternary chalcogenides of $Cu_2CdSnSe_4$ *Adv. Mater.* **21** 3808–12
[23] Vaney J-B, Yamini S A, Takaki H, Kobayashi K, Kobayashi N and Mori T 2019 Magnetism-mediated thermoelectric performance of the Cr-doped bismuth telluride tetradymite *Mater. Today Phys.* **9** 100090
[24] Ahmed F, Tsujii N and Mori T 2017 Thermoelectric properties of $CuGa_{1-x}Mn_xTe_2$: power factor enhancement by incorporation of magnetic ions *J. Mater. Chem.* A **5** 7545–54
[25] Xiao C, Li K, Zhang J, Tong W, Liu Y, Li Z, Huang P, Pan B, Su H and Xie Y 2014 Magnetic ions in wide band gap semiconductor nanocrystals for optimized thermoelectric properties *Mater. Horiz.* **1** 81–86
[26] Song Q, Qiu P, Hao F, Zhao K, Zhang T, Ren D, Shi X and Chen L 2016 Quaternary pseudocubic $Cu_2TMSnSe_4$ (TM = Mn, Fe, Co) chalcopyrite thermoelectric materials *Adv. Electron. Mater.* **2** 1600312
[27] Tsujii N and Mori T 2013 High thermoelectric power factor in a carrier-doped magnetic semiconductor $CuFeS_2$ *Appl. Phys. Express* **6** 043001
[28] Hamajima T, Kambara T, Gondaira K I and Oguchi T 1981 Self-consistent electronic structures of magnetic semiconductors by a discrete variational $X\alpha$ calculation. III. Chalcopyrite $CuFeS_2$ *Phys. Rev.* B **24** 3349
[29] Larson A C and von Dreele R B 1994 GSAS. Report LAUR 86–748
[30] Cowan R D 1963 Pulse method of measuring thermal diffusivity at high temperatures *J. Appl. Phys.* **34** 926–7
[31] Quintero M, Tovar R, Barreto A, Quintero E, Rivero A, Gonzalez J, Porras G S, Ruiz J, Bocaranda P and Broto J 1998 Crystallographic and magnetic properties of $Cu_2FeGeSe_4$ and $Cu_2FeGeTe_4$ compounds *Phys. Status Solidi* b **209** 135–43
[32] Chetty R, Bali A, Femi O E, Chattopadhyay K and Mallik R C 2016 Thermoelectric properties of In-doped $Cu_2ZnGeSe_4$ *J. Electron. Mater.* **45** 1625–32
[33] Shannon R D 1976 Revised effective ionic-radii and systematic studies of interatomic distances in halides and chalcogenides *Acta Crystallogr.* A **32** 751–67
[34] Raju C, Falmbigl M, Rogl P, Yan X, Bauer E, Horky J, Zehetbauer M and Chandra Mallik R 2013 Thermoelectric properties of chalcogenide based $Cu_{2+x}ZnSn_{1-x}Se_4$ *AIP Adv.* **3** 032106
[35] Scragg J J S, Choubrac L, Lafond A, Ericson T and Platzer-Bjorkman C 2014 A low-temperature order-disorder transition in Cu_2ZnSnS_4 thin films *Appl. Phys. Lett.* **104** 041911
[36] Huang D and Persson C 2013 Band gap change induced by defect complexes in Cu_2ZnSnS_4 *Thin Solid Films* **535** 265–9
[37] Rey G, Weiss T P, Sendler J, Finger A, Spindler C, Werner F, Melchiorre M, Hála M, Guennou M and Siebentritt S 2016 Ordering kesterite improves solar cells: a low temperature post-deposition annealing study *Sol. Energy Mater. Sol. Cells* **151** 131–8
[38] Rey G, Redinger A, Sendler J, Weiss T P, Thevenin M, Guennou M, El Adib B and Siebentritt S 2014 The band gap of $Cu_2ZnSnSe_4$: effect of order-disorder *Appl. Phys. Lett.* **105** 112106
[39] Mangelis P, Vaqueiro P, Smith R I and Powell A V 2021 The onset of copper-ion mobility and the electronic transitions in kesterite, $Cu_2ZnGeSe_4$ *J. Mater. Chem.* A **9** 27493–502

[40] Ottenburgs R and Goethals H 1972 Synthèse et polymorphisme de la briartite *Bull. Soc. Fr. Minéral Cristallogr.* **95** 458–63
[41] Song Q, Qiu P, Chen H, Zhao K, Guan M, Zhou Y, Wei T-R, Ren D, Xi L and Yang J 2018 Enhanced carrier mobility and thermoelectric performance in $Cu_2FeSnSe_4$ diamond-like compound via manipulating the intrinsic lattice defects *Mater. Today Phys.* **7** 45–53
[42] Zeier W G, LaLonde A, Gibbs Z M, Heinrich C P, Panthöfer M, Snyder G J and Tremel W 2012 Influence of a nano phase segregation on the thermoelectric properties of the p-type doped stannite compound $Cu_{2+x}Zn_{1-x}GeSe_4$ *J. Am. Chem. Soc.* **134** 7147–54